Heliyon 10 (2024) e39909

Contents lists available at ScienceDirect

Heliyon

journal homepage: www.cell.com/heliyon

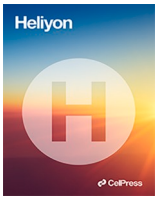

Research article

Bioinformatics *in vivo* and *in vitro* assays identified miR-486-5p as a tumor suppressor miRNA in hepatocellular carcinoma

Xiang Li [a,b,1], Jie Fang [c,1], Xueyan Huang [a], Yeqi Wu [d], Rui Wang [a,*]

[a] Hangzhou TCM Hospital Affiliated to Zhejiang Chinese Medical University, Hangzhou, Zhejiang, China
[b] Department of Immunology, School of Basic Medicine, Tongji Medical College, Huazhong University of Science & Technology, Hubei, Wuhan, China
[c] Zhejiang Provincial Laboratory of Experimental Animal's & Nonclinical Laboratory Studies, Hangzhou Medical College, Hangzhou, Zhejiang, China
[d] The First Affiliated Hospital of Zhejiang Chinese Medical University, Hangzhou, Zhejiang, China

ARTICLE INFO

Keywords:
miR-486-5p
SRSF3
Hepatocellular carcinoma
TCGA
GEO

ABSTRACT

Background: This study aimed to explore key microRNAs (miRNAs) and their effects on hepatocellular carcinoma (HCC) progression.
Methods: Key deregulated miRNAs in HCC were screened from The Cancer Genome Atlas (TCGA) and Gene Expression Omnibus (GEO) databases. The anti-cancer effects of miR-486-5p were validated using a cell counting kit-8 assay, flow cytometry, scratch assay, transwell assay, and an orthotopic transplantation tumor model. Furthermore, the expression, clinical significance, and function of miR-486-5p and its targets were predicted using bioinformatics. Additionally, a luciferase reporter assay was performed to validate the miR-486-5p target.
Results: By integrating multiple datasets from TCGA and GEO databases, we identified miR-486-5p as the only lowly expressed miRNA in HCC, whose expression was also associated with clinical features. Additionally, miR-486-5p exhibited anti-cancer properties both *in vitro* and *in vivo*. Ser/Arg-rich splicing factor 3 (SRSF3) was the predicted target of miR-486-5p, and this finding was further supported by correlation analysis, quantitative polymerase chain reaction, and luciferase reporter assays. Furthermore, *SRSF3* expression was upregulated, and high *SRSF3* expression was correlated with poor survival in patients with HCC. According to Gene Ontology, Kyoto Encyclopedia of Genes and Genomes, and Gene Set Enrichment Analysis, SRSF3 promotes cancer-related pathways.
Conclusion: miR-486-5p suppresses cancer progression in HCC by interacting with SRSF3. Therefore, miR-486-5p and SRSF3 may serve as promising therapeutic targets for HCC treatment.

1. Introduction

Hepatocellular carcinoma (HCC) is the fourth most common cause of tumor-related death worldwide, with a 5-year recurrence rate of 40%–70 %, even after surgical resection, liver transplantation, and tumor immune-targeted therapy [1,2]. Understanding the molecular mechanisms underlying HCC and identifying novel therapeutic targets are imperative to improving patient outcomes.

MicroRNAs (miRNAs), small non-coding RNA molecules, regulate gene expression by binding to the 3′ UTR of target mRNAs, thereby inhibiting translation or degradation of the target mRNA [3]. They are involved in various biological processes including cell

* Corresponding author.
E-mail address: hzszyywr@126.com (R. Wang).
[1] These authors contributed equally to this work.

https://doi.org/10.1016/j.heliyon.2024.e39909
Received 31 August 2023; Received in revised form 8 August 2024; Accepted 27 October 2024
Available online 29 October 2024

proliferation, differentiation, apoptosis, and the cell cycle [4]. Dysregulation of miRNAs is common in numerous human diseases such as Alzheimer's disease [5], heart failure [6], and various cancers [7], including HCC [8]. Moreover, miRNAs play critical roles in tumor progression and serve as potential biomarkers for cancer diagnosis and treatment [9].

Recent advancements in microarray and high-throughput sequencing technologies have facilitated the screening of molecular markers and the study of molecular mechanisms in malignant cancers [10]. Among these, miR-486-5p has emerged as a significant player in various cancers; however, its role in HCC remains unclear. Notably, miR-486-5p functions as a tumor suppressor in several cancers, including lung, colorectal, and breast cancers [11–13]. However, its specific roles and regulatory mechanisms in HCC have not been fully elucidated.

In this study, we used bioinformatic tools to analyze gene expression profiles from The Cancer Genome Atlas (TCGA) and GSE36915, GSE21362, and GSE74618 microarrays from the Gene Expression Omnibus (GEO) database. Our findings identified miR-486-5p as a crucial miRNA associated with HCC development. Subsequently, we predicted and validated its target using *in vitro* and *in vivo* assays. Our findings may help identify a prognostic biomarker and potential therapeutic target for HCC.

2. Materials and methods

2.1. Data source

Gene expression profiles were extracted from public datasets of liver cancer and normal liver tissues, including TCGA-Liver Hepatocellular Carcinoma Collection (LIHC) (containing 375 HCC and 50 normal samples), GSE36915 (containing 61 HCC, 21 normal, 26 high-grade, and 26 low-grade samples), GSE21362 (containing 73 HCC and 73 normal samples), GSE74618 (containing 230 HCC and 10 normal samples), and the Clinical Proteomic Tumor Analysis Consortium (CPTAC) HCC (containing 165 HCC and 165 normal samples). The data were normalized and presented in log2 format. The clinical information of patients with HCC was downloaded from TCGA-LIHC dataset.

2.2. Key miRNA screening

The DESeq2 package [14] was used to analyze differentially expressed miRNAs (DEMs) between normal and HCC tissues based on RNA-seq data from TCGA-LIHC dataset. To further improve prediction accuracy, datasets GSE36915, GSE21362, and GSE74618 from the GEO database were collected. DEMs were filtered from the normalized microarray data using the limma package [15]. The screening thresholds for DEM were logFC ≤ -0.8 and adj.p.val <0.05. Common DEMs among these datasets were regarded as key miRNAs.

2.3. Correlation between miR-486-5p/SRSF3 expression and clinical variables

The mRNA expression of miR-486-5p and *SRSF3* among the different clinical features was analyzed and visualized using the ggplot2 package. Additionally, samples in TCGA-LIHC dataset were divided into high- and low-expression groups based on the median miR-486-5p/*SRSF3* expressions. The $\chi 2$ or Fisher's exact test was used to determine statistical differences between the groups. Moreover, data regarding SRSF3 expression in HCC was downloaded from the UALCAN database [16].

2.4. Clinical significance of miR-486-5p/SRSF3

To evaluate the diagnostic value of miR-486-5p/SRSF3 in TCGA-LIHC datasets, the receiver operating characteristic (ROC) curve was plotted using the pROC package [17]. Cox regression was used to assess the prognosis of miR-486-5p/SRSF3, and the survival package was used to analyze the survival of patients with HCC. Survival curves were visualized using the SurvMiner package. The prognostic value of miR-486-5p in patients with HCC was investigated using univariate and multivariate Cox regression analyses. Variables that displayed statistical significance or clinical relevance in the univariate analysis were selected in the multivariate Cox analysis. Additionally, highly correlated variables were excluded to prevent model instability due to multicollinearity. Furthermore, the KMplotter database was used to determine the overall survival of patients with liver cancer split by the best cutoff based on miR-486-5p expression. The predictive efficacy of SRSF3 for survival was confirmed based on the time-dependent ROC curves using the timeROC package.

2.5. miR-486-5p function prediction

The potential targets of miR-486-5p were searched in the miRTarBase 2020 database [18], and their functions were predicted using Kyoto Encyclopedia of Genes and Genomes (KEGG) enrichment analysis of miR-486-5p targets using the clusterProfiler package [19].

2.6. Cell lines and cell transfection

All cell lines were obtained from the American Type Culture Collection (Manassas, VA, USA). The normal liver cell line LO2 was cultured in RPMI-1640 medium (R8758, Sigma) containing 10 % fetal bovine serum (FBS) (10437-028, Gibco). The liver cancer cell line HepG2 was cultured in minimum essential medium (M4655, Sigma) containing 10 % FBS. LM3, Huh7, and 97H cells were cultured

in Dulbecco's Modified Eagle's medium (D6429; Sigma) supplemented with 10 % FBS. All cell lines were maintained in incubators at 37 °C and 5 % CO2. After 2–3 days of culture, the cells were digested with trypsin, passaged, and cultured until they reached the log phase of growth. Cells exhibiting optimal growth rates, characterized by a high proliferation index and minimal cell death, were selected for subsequent experiments.

To overexpress or inhibit miR-486-5p, HCC cells were transfected with either a miR-486-5p mimic or an inhibitor using Lipofectamine 2000 (11668-027, Invitrogen) following the manufacturer's protocol. Each experiment was performed thrice, with six replicate wells for each experimental group.

2.7. Quantitative polymerase chain reaction (qPCR)

Total RNA was extracted from cells and HCC tissues using TRIzol reagent (Invitrogen), and its concentration was determined using a spectrophotometer (Eppendorf). Primerscript RT reagent kit (TaKaRa) was used for reverse transcription at 37 °C for 15 min and 85 °C for 5 s qPCR was performed using SYBR Premix Ex Taq (TaKaRa) on a real-time PCR instrument (LC480, Roche) following the manufacturer's instructions. U6 snRNA or GAPDH was used as an internal reference. Reaction conditions were set at 95 °C for 10 min, 40 cycles at 95 °C for 15 s, 60 °C for 30 s, and 72 °C for 42 s. All experiments were repeated thrice. The $2^{-\Delta\Delta CT}$ method was used to calculate the relative expressions of miR-486-5p and SRSF3. The primer sequences are listed in Table S1.

2.8. Cell counting kit-8 (CCK-8)

The cells were seeded into 96-well plates (3599, Corning) at a density of 5×10^4 cells/mL. Specifically, 100 μL of the cell suspension was added to each well, resulting in 5000 cells per well. CCK-8 (CK04, Dojindo) assay was performed after 1, 2, 3, 4, and 5 days of incubation, and absorbance was detected at 450 nm using a microplate reader (ELX808, BIOTeck). Three replicate wells were used for each group.

2.9. Flow cytometry

The cells in each group were collected via trypsin (25200-072, Gibco) digestion and centrifugation at 4 °C. The Annexin V-FITC/PI Apoptosis Detection Kit I (556547, BD) and flow cytometry (Gallios, Beckman Gallios) were used to detect apoptosis. The experiment was repeated thrice.

2.10. Scratch assay

Liver cancer cell lines were seeded in six-well plates (703001, NEST) at a certain density to enable them to reach approximately 80 % confluence. Cells were scraped using a sterile pipette tip to create scratches. The cells were uniformly distributed in the well before seeding to ensure the homogeneous distribution of cells around the scratch area, and a scratch was made with consistent pressure and speed. The initial scratch width was measured using an inverted microscope (CKX41, Olympus). The scratch width was measured again after 48 h, and the migration rate was calculated by comparing the initial and final scratch widths.

2.11. Transwell invasion assay

The cells were starved in serum-free medium for 12 h prior to the assay. The 24-well transwell units (3422, Corning) were precoated with Matrigel (354248, BD) and hydrated for 2 h in an incubator (311, Thermo) with 500 μL of serum-free media pre-warmed to 37 °C. The lower chambers were filled with a medium containing 10 % FBS to serve as a chemoattractant. The cells were digested with 0.25 % trypsin (25200-072, Gibco) and seeded in the upper chambers at a density of 1×10^5 cells/well. The cells were then cultured in an incubator at 37 °C and 5 % CO2. The non-invading cells on the upper surface were removed using a cotton swab after 24 h. Invasive cells on the lower surface of the membrane were fixed with 4 % paraformaldehyde (G-1002, Servicebio) for 20 min at room temperature and stained with 0.1 % crystal violet solution (CO528-25g, Sangon) for 10 min. Five fields were randomly selected to count invasive cells under a microscope (CKX41, Olympus).

2.12. Establishment of an in situ HCC mouse model and in vivo imaging

Twenty male SPF/Balb/c nude mice, aged 4–5 weeks and weighing 18 ± 2 g, were obtained from the Laboratory Animal Center of Hangzhou Medical College. The mice were individually housed in an air-conditioned room maintained at 20–25 °C and 40–70 % humidity under a 12:12 h light/dark cycle, with free access to food and water. Mice were divided into two groups of 10 mice each. HepG2 cells (SCSP-510, Chinese Academy of Sciences) were transfected with either a negative control (NC) or miR-486-5p lentivirus (packed with luciferase; Hanyinbt). The exact number of viable cells was determined using a hemocytometer and trypan blue exclusion assay before mixing with a Matrigel matrix (354248, Corning) in a 1:1 ratio in an ice bath. Subsequently, 50 μL of the mixture containing approximately 1 million viable cells was injected under the liver envelope of each mouse. On day 2 post-modeling, each mouse was intraperitoneally injected with 200 μL of D-luciferin (15 mg/mL potassium salt solution, 40902ES02, Yeasen). The mice were anesthetized with isoflurane gas (R510-22-10, RWD Life Science Co., Ltd.) after 10 min via an isoflurane vaporizer (RC2, Vetequip, USA) and subjected to *in vivo* imaging using the IVIS Lumina LT system (PerkinElmer) to observe tumor cell growth. Mice from both

groups with similar fluorescence values were selected for imaging on days 5, 11, and 17. The mice were sacrificed on day 17, and their tumor tissues were collected for further analysis. All experimental procedures were approved by the Institutional Animal Care and Use Committee (IACUC) of ZJCLA (ZJCLA-IACUC-20110044) and complied with the Chinese guidelines for the care and use of animals. Additionally, all animal studies were performed in accordance with the ARRIVE guidelines.

2.13. Hematoxylin–eosin (HE) staining

HCC tissues were embedded in paraffin and sectioned as described previously [20]. Finally, the sections were sealed and examined under a microscope.

2.14. Immunohistochemical (IHC) staining

HCC tissues were fixed in 10 % neutral-buffered formalin, embedded in paraffin (69018961, Sinopharm Chemical Reagent Co., Ltd.), and sliced into 4-μm-thick sections. The sections were dewaxed in xylene (10023418, Sinopharm Chemical Reagent Co., Ltd.) and rehydrated using a graded series of alcohol solutions (10092680, Sinopharm Chemical Reagent Co., Ltd.). Antigen retrieval was performed by heating the sections in ethylenediaminetetraacetic acid buffer (pH 8.0) in a microwave oven for 15 min at medium power. The sections were then incubated with 3 % hydrogen peroxide (H_2O_2) solution (10011218, Sinopharm Chemical Reagent Co., Ltd.) for 25 min at room temperature to quench endogenous peroxidase activity, followed by blocking with 3 % bovine serum albumin for 30 min at room temperature to prevent non-specific binding. The sections were then incubated overnight with primary antibodies, either mouse anti-human PCNA antibody (ab29, Abcam) or rabbit anti-human Ki67 antibody (27309-1-AP, Proteintech), at 4 °C. The next day, sections were incubated with a horseradish peroxidase-labeled broad-spectrum secondary antibody (D-3004; Longisland Biotech) for 50 min at room temperature. Detection was performed using 3,3′-Diaminobenzidine tetrahydrochloride (FL-6001, Longsland Biotech) as the chromogen, followed by counterstaining with hematoxylin (714094, BASO). The sections were then dehydrated, cleared, and mounted using a neutral resin (G8590; Solarbio). Immunoreactivity was then evaluated, and images were captured using a microscope (CX41, OLYMPUS) at 100 × magnification for randomly selected fields.

2.15. miR-486-5p target prediction

miR-486-5p targets were predicted by the intersection of the obtained genes from the three approaches, including the top 10 targets collected from the TargetScan and miRWalk databases and hub genes in TCGA-LIHC dataset. The correlation between miR-486-5p expression and SRSF3 was analyzed using Pearson's method.

2.16. Luciferase reporter assay

The 3′ UTR region of SRSF3 was engineered into wild-type and mutant luciferase reporter vectors, pmirGLO-h. SRSF3-3UTR-WT (BK625, Umibio, Shanghai, China) and pmirGLO-h. SRSF3-3UTR-MU (BK626; Umibio). The miR-486-5p mimic and sea kidney internal reference plasmid pRL were co-transfected into HepG2 cells using X-tremegene HP transfection reagent (06366236001, ROCHE). The cells were lysed, and supernatants were collected after 36 h of transfection. Luciferase activity of HepG2 cells was detected using the Dual-Luciferase® Reporter Assay System (E1910, Promega) and a microplate reader (Synergy HT, BioTek) following the manufacturer's instructions. The firefly luciferase activity, normalized to the sea kidney luciferase activity, was measured as relative luciferase activity. The experiment was repeated thrice.

2.17. Gene Ontology (GO) and KEGG enrichment analysis

The samples in TCGA-LIHC dataset were divided into two groups based on the median SRSF3 expression. DEGs between the groups were filtered and annotated using GO [21] and KEGG [22] enrichment analyses using the clusterProfiler package [19]. GO enrichment analysis was performed for biological processes (BP), cellular components (CC), and molecular functions (MF). The results were presented as bubble charts.

2.18. Gene Set Enrichment Analysis (GSEA)

Tumor samples were divided into SRSF3 low- and high-expression groups based on TCGA-LIHC dataset, and differential analysis was performed. The c2.cp.kegg.v5.1.symbols.gmt gene set was obtained from the MsigDB database [23] and subjected to GSEA with 1000 random permutations. An adjusted $p < 0.05$ was identified as significant enrichment.

2.19. Immune infiltrate analysis

Immune cell subsets in HCC tissues were calculated using the single-sample GSEA algorithm of the GSVA package [24]. The relationship between miR-486-5p/SRSF3 expression and the immune cell fraction is illustrated in boxplots and lollipop charts.

2.20. Statistical analysis

R (version 3.6.3) was used for statistical analysis. Normally distributed data were expressed as the mean ± standard deviation, and *t*-test was employed to compare differences between two groups. Non-normally distributed data were expressed as median (interquartile range), and Mann–Whitney U and Kruskal–Wallis H tests were employed to compare differences between two groups and multiple groups, respectively. Numerical data were compared using $\chi 2$ test or Fisher's exact test between the two groups. The correlation between the two variables was measured using Pearson's method. Statistical significance was set at $p < 0.05$.

3. Results

3.1. Key tumor suppressor miRNAs in HCC screened from TCGA and GEO databases

miR-486-5p was commonly downregulated in all datasets downloaded in this study, including TCGA-LIHC, GSE36915, GSE21362, and GSE74618 (Fig. 1A B). Furthermore, we determined miR-486-5p expression in TCGA-LIHC dataset (Table 1). miR-486-5p was downregulated in both unpaired (Fig. 1C; 375 HCC and 50 normal samples) and paired tumor tissues (Fig. 1D; 49 HCC and 49 normal samples). Moreover, its expression was further reduced in patients with HCC with several clinical features, including tumor (Fig. 1E; 202 tumor-free, 153 tumor, and 50 normal samples), T2 (Fig. 1F; 183 T1, 95 T2, and 50 normal samples), M1 stage (Fig. 1G; 268 M0, 4 M1, and 50 normal samples), higher pathologic stage (Fig. 1H; 173 stage I, 87 stage II, 85 stage III, and 50 normal samples), higher histologic grade (Fig. 1I; 55 G1, 178 G2, 124 G3, and 50 normal samples), Child-Pugh grade B (Fig. 1J; 219 A, 21 B, and 50 normal

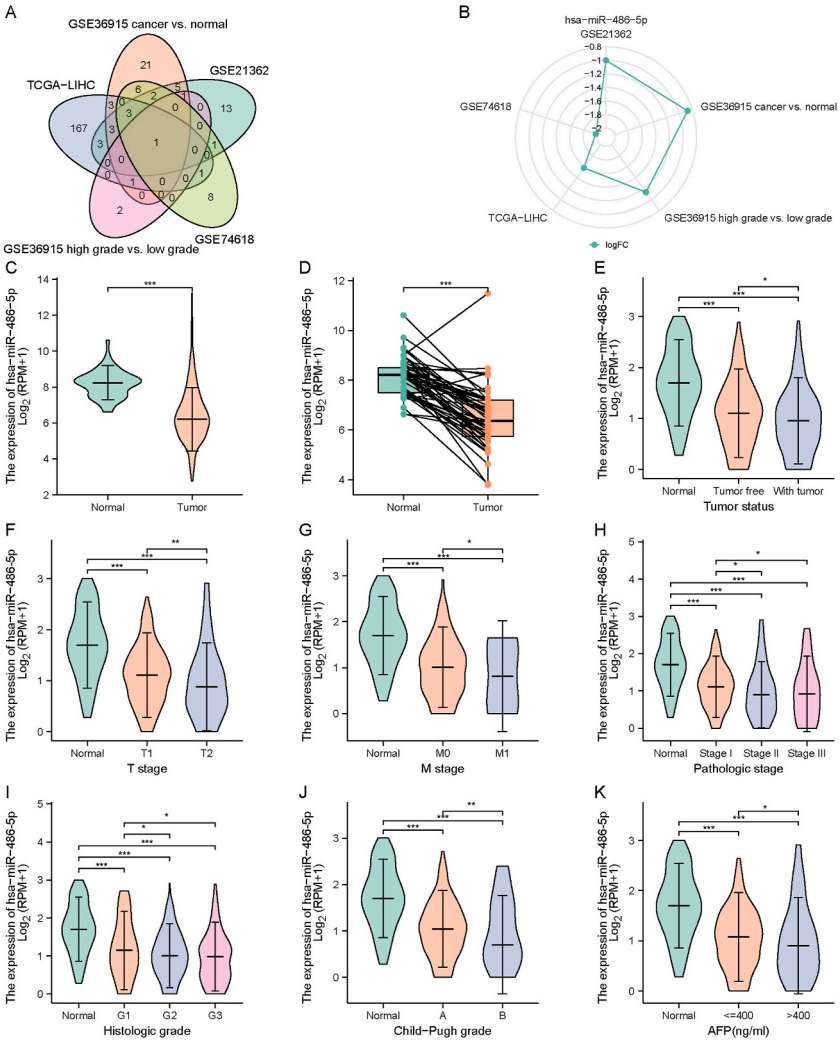

Fig. 1. miR-486-5p expression in HCC.
(A) Downregulated miRNAs in various datasets. (B) Fold-change in miR-486-5p expression among various datasets. (C–K) Correlation between miR-486-5p expression and clinical characteristics in TCGA-LIHC dataset. *$p < 0.05$; **$p < 0.01$; ***$p < 0.001$.

Table 1
Correlation between miR-486-5p and clinicopathologic characteristics in patients with HCC.

Characteristic	Low expression of hsa-miR-486-5p	High expression of hsa-miR-486-5p	p-value
N	187	188	
T stage, n (%)			0.625
T1	92 (24.7 %)	92 (24.7 %)	
T2	50 (13.4 %)	45 (12.1 %)	
T3	36 (9.7 %)	44 (11.8 %)	
T4	8 (2.2 %)	5 (1.3 %)	
N stage, n (%)			1.000
N0	125 (48.1 %)	131 (50.4 %)	
N1	2 (0.8 %)	2 (0.8 %)	
M stage, n (%)			1.000
M0	138 (50.2 %)	133 (48.4 %)	
M1	2 (0.7 %)	2 (0.7 %)	
Pathologic stage, n (%)			0.877
Stage I	85 (24.2 %)	89 (25.4 %)	
Stage II	45 (12.8 %)	42 (12 %)	
Stage III	40 (11.4 %)	45 (12.8 %)	
Stage IV	3 (0.9 %)	2 (0.6 %)	
Tumor status, n (%)			0.965
Tumor free	102 (28.7 %)	100 (28.1 %)	
With tumor	79 (22.2 %)	75 (21.1 %)	
Gender, n (%)			0.972
Female	60 (16 %)	59 (15.7 %)	
Male	127 (33.9 %)	129 (34.4 %)	
Race, n (%)			0.425
Asian	87 (24 %)	76 (20.9 %)	
Black or African American	7 (1.9 %)	10 (2.8 %)	
White	87 (24 %)	96 (26.4 %)	
Age, n (%)			0.682
≤60	91 (24.3 %)	87 (23.3 %)	
>60	95 (25.4 %)	101 (27 %)	
Weight, n (%)			0.349
≤70	97 (28 %)	90 (25.9 %)	
>70	74 (21.3 %)	86 (24.8 %)	
Height, n (%)			0.729
< 170	102 (29.7 %)	99 (28.8 %)	
≥170	69 (20.1 %)	74 (21.5 %)	
BMI, n (%)			0.227
≤25	95 (27.9 %)	85 (25 %)	
>25	73 (21.5 %)	87 (25.6 %)	
Residual tumor, n (%)			0.082
R0	157 (45.4 %)	171 (49.4 %)	
R1	12 (3.5 %)	5 (1.4 %)	
R2	0 (0 %)	1 (0.3 %)	
Histologic grade, n (%)			0.042
G1	18 (4.9 %)	37 (10 %)	
G2	91 (24.5 %)	86 (23.2 %)	
G3	68 (18.3 %)	58 (15.6 %)	
G4	8 (2.2 %)	5 (1.3 %)	
AFP(ng/mL), n (%)			0.656
≤400	113 (39.9 %)	105 (37.1 %)	
>400	31 (11 %)	34 (12 %)	
Adjacent hepatic tissue inflammation, n (%)			0.076
None	53 (22.2 %)	66 (27.6 %)	
Mild	61 (25.5 %)	41 (17.2 %)	
Severe	9 (3.8 %)	9 (3.8 %)	
Albumin(g/dl), n (%)			0.373
<3.5	31 (10.3 %)	39 (12.9 %)	
≥3.5	119 (39.4 %)	113 (37.4 %)	
Prothrombin time, n (%)			0.291
≤4	111 (37.1 %)	101 (33.8 %)	
>4	39 (13 %)	48 (16.1 %)	
Child-Pugh grade, n (%)			0.213
A	116 (47.5 %)	106 (43.4 %)	
B	8 (3.3 %)	13 (5.3 %)	
C	0 (0 %)	1 (0.4 %)	
Fibrosis ishak score, n (%)			0.247
0	33 (15.1 %)	43 (19.7 %)	
1/2	17 (7.8 %)	13 (6 %)	

(*continued on next page*)

Table 1 (*continued*)

Characteristic	Low expression of hsa-miR-486-5p	High expression of hsa-miR-486-5p	p-value
3/4	19 (8.7 %)	11 (5 %)	
5/6	44 (20.2 %)	38 (17.4 %)	
Vascular invasion, n (%)			0.439
No	113 (35.3 %)	95 (29.7 %)	
Yes	55 (17.2 %)	57 (17.8 %)	

samples), and higher alpha-fetoprotein (AFP) (Fig. 1K; 215 with ≤400, 65 with >400, and 50 normal samples). Except for these, no difference was observed in miR-486-5p expression among patients with different adjacent hepatic tissue inflammation (Fig. S1A), age (Fig. S1B), albumin level (Fig. S1C), BMI (Fig. S1D), fibrosis ishak score (Fig. S1E), sex (Fig. S1F), height (Fig. S1G), prothrombin time (Fig. S1H), race (Fig. S1I), residual tumor (Fig. S1J), vascular invasion (Fig. S1K), and weight (Fig. S1L).

3.2. Clinical significance of miR-486-5p

In TCGA-LIHC dataset, the ROC curve showed an AUC of 0.857, indicating that miR-486-5p expression could differentiate patients with HCC from healthy individuals (Fig. 2A). In terms of survival, lower miR-486-5p expression predicted poorer overall survival (Fig. 2B) and disease-free survival (Fig. 2C) in TCGA-LIHC dataset. Furthermore, we analyzed the prognostic value of miR-486-5p in a cohort of 166 patients with liver cancer obtained from the KMplotter database. The median overall survival of patients with liver cancer with high miR-486-5p expression was 70 months, whereas that of patients with low miR-486-5p expression was 34 months (Fig. 2D). To evaluate the independent prognostic significance of miR-486-5p on overall survival in hepatocellular carcinoma patients, we have conducted both univariate and multivariate Cox regression analyses in TCGA-LIHC dataset (Figs. S2 and S3). The multivariate analysis confirms that the expression level of hsa-miR-486-5p remains a significant prognostic factor for overall survival, even after adjusting for other clinical variables.

3.3. Tumor suppressive effects of miR-486-5p

miR-486-5p targets determined from the miRTarbase website were involved in HCC and cancer-related pathways (Fig. S4). Subsequently, we validated miR-486-5p expression in various HCC cell lines and the hepatocyte cell line LO2. Notably, miR-486-5p

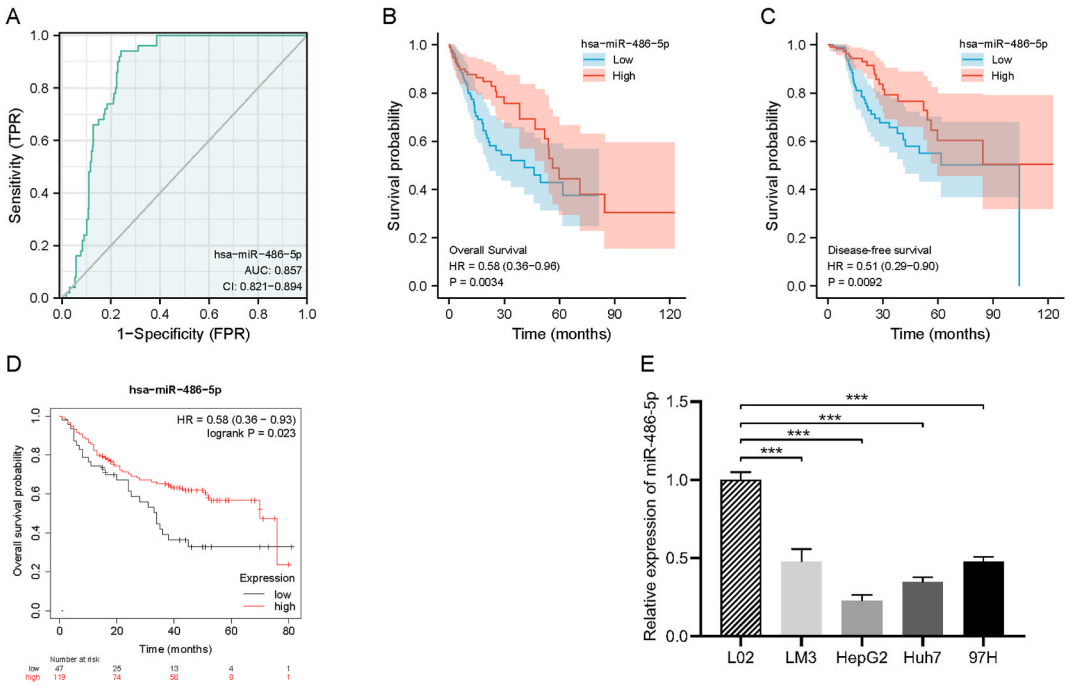

Fig. 2. Clinical significance and expression of miR-486-5p in HCC cells.
(A) The diagnostic value of miR-486-5p evaluated based on the ROC curve. (B) The effect of miR-486-5p on overall survival evaluated using Cox regression in TCGA-LIHC dataset. (C) The effect of miR-486-5p on disease-free survival evaluated using Cox regression in TCGA-LIHC dataset. (D) The effect of miR-486-5p on overall survival evaluated using the log-rank test in the KMplotter database. (E) The expression of miR-486-5p in HCC cells. ***p < 0.001.

expression was lower in HCC cells than in LO2 cells, particularly in HepG2 and Huh7 cells (Fig. 2E). We overexpressed miR-486-5p in these two cell lines (Fig. 3A). The growth curves of the CCK-8 assay (Fig. 3B and C) revealed that the miR-486-5p mimic inhibited the viability and proliferation of HepG2 and Huh7 cells. In contrast, apoptosis of HepG2 and Huh7 cells was enhanced after transfection with the miR-486-5p mimic (Fig. 3D and E). In addition, HepG2 and Huh7 cells transfected with the miR-486-5p mimic showed weaker migration (Fig. 3F and G) and invasion (Fig. 3H and I) abilities. Furthermore, LM3 and 97H cells were transfected with an miR-486-5p inhibitor (Fig. 4A). The growth curves of the CCK-8 assay (Fig. 4B and C) demonstrated that the miR-486-5p inhibitor promoted the viability and proliferation of LM3 and 97H cells, respectively. In contrast, the apoptosis in LM3 and 97H cells decreased after transfection with the miR-486-5p inhibitor (Fig. 4D and E). Additionally, LM3 and 97H cells transfected with the miR-486-5p inhibitor exhibited increased migration (Fig. 4F and G) and invasion (Fig. 4H and I).

3.4. *miR-486-5p inhibited HCC growth in vivo*

To test the anti-cancer activity of miR-486-5p *in vivo*, we constructed an in situ transplantation tumor model using nude mice by injecting HepG2 cells into the liver envelope. *In vivo* imaging revealed that miR-486-5p suppressed HCC growth (Fig. 5A and B). Thereafter, we isolated HCC tissues and performed HE staining (Fig. 5C). qPCR results demonstrated that miR-486-5p was overexpressed (Fig. 5D). Furthermore, higher PCNA (Fig. 5E) and Ki67 (Fig. 5F) protein expression was observed in the miR-486-5p overexpression group using IHC.

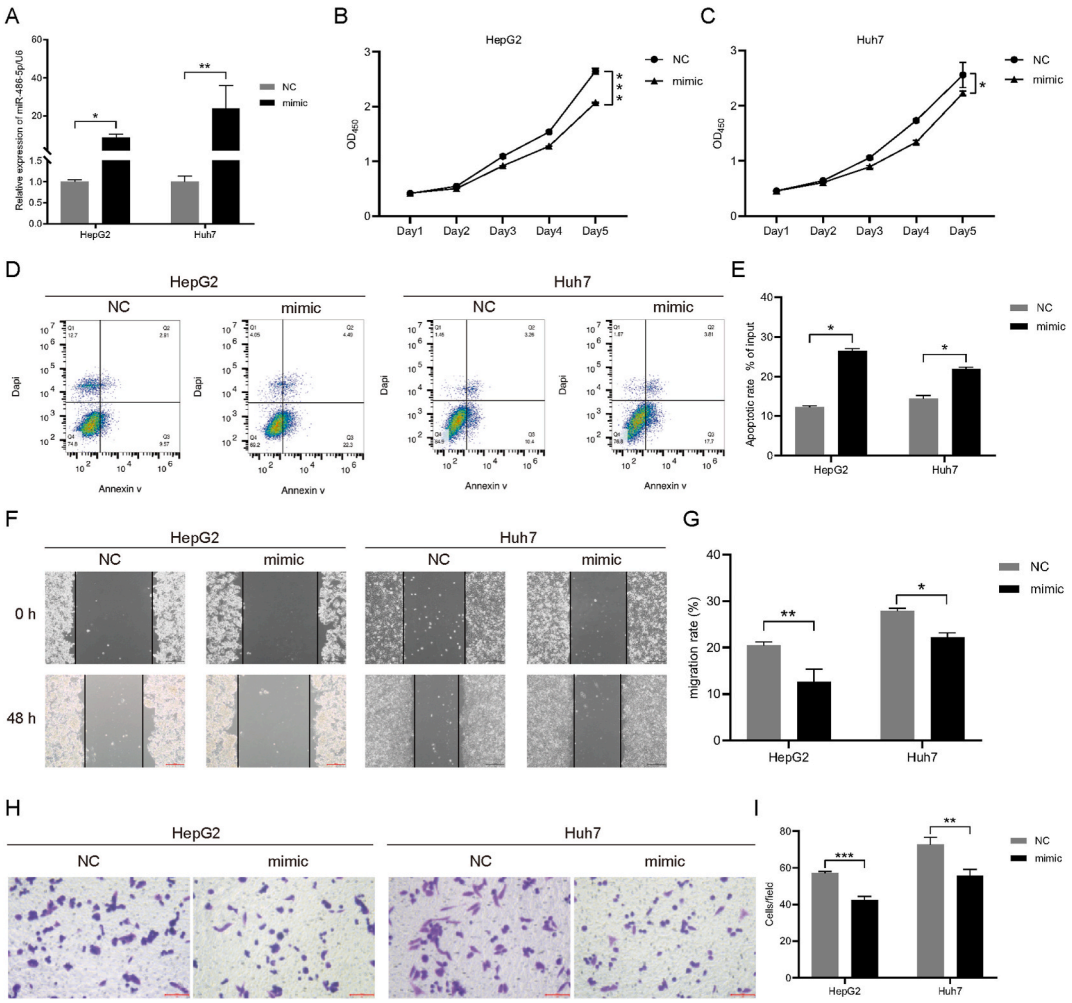

Fig. 3. miR-486-5p overexpression inhibited HCC cell proliferation, migration, and invasion.
HCC cells were transfected with the miR-486-5p mimic. (A) miR-486-5p expression after transfection with the miR-486-5p mimic. (B) Viability of HepG2 cells detected using the CCK-8 assay. (C) Viability of Huh7 cells detected using the CCK-8 assay. (D, E) Apoptosis in HCC cells detected using flow cytometry. (F, G) Migration of HCC cells detected using the scratch test. (H, I) Invasion of HCC cells detected using a transwell assay. *$p < 0.05$; **$p < 0.01$; ***$p < 0.001$.

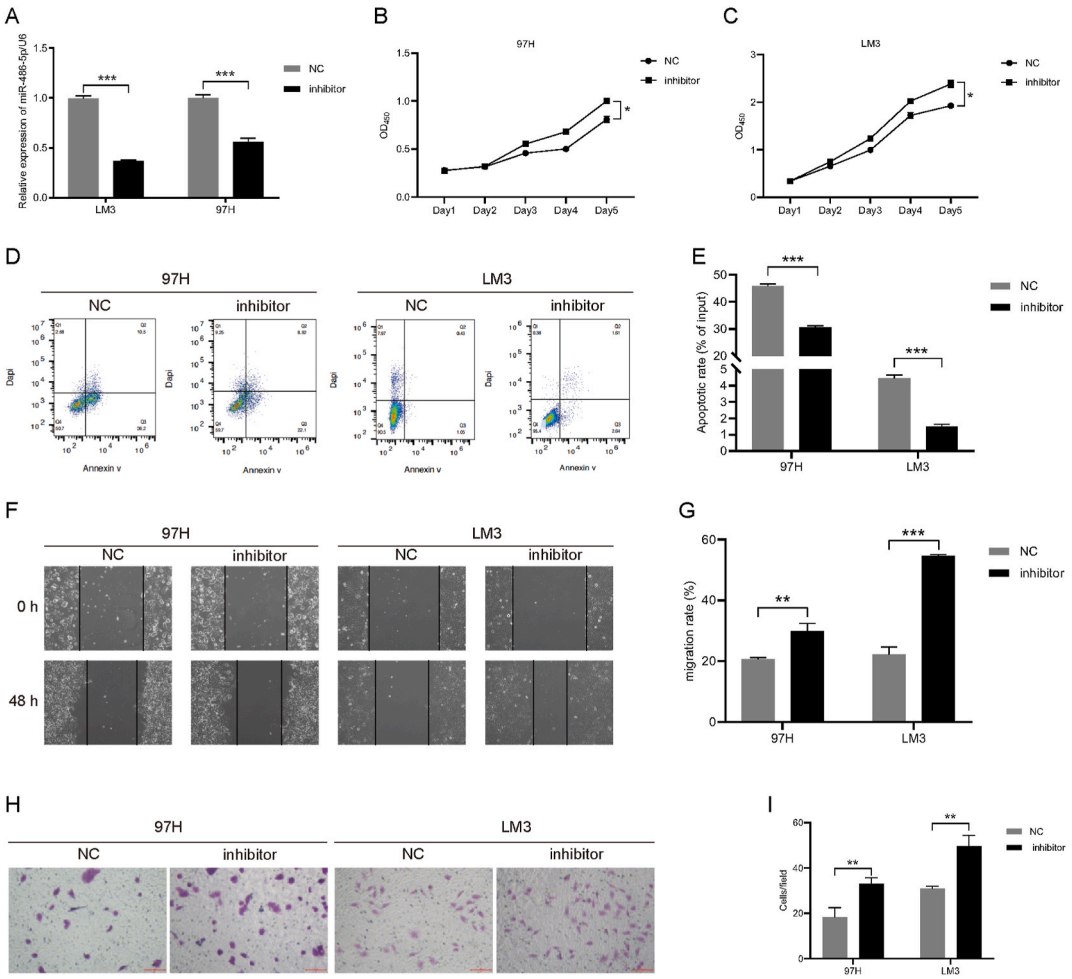

Fig. 4. miR-486-5p silencing promoted HCC cell proliferation, migration, and invasion.
HCC cells were transfected with the miR-486-5p inhibitor. (A) miR-486-5p expression after transfection with an miR-486-5p inhibitor. (B) Viability of 97H cells detected using the CCK-8 assay. (C) Viability of LM3 cells as detected using the CCK-8 assay. (D, E) Apoptosis of HCC cells detected using flow cytometry. (F, G) Migration of HCC cells detected using the scratch test. (H, I) Invasion of HCC cells detected using a transwell assay. *$p < 0.05$; **$p < 0.01$; ***$p < 0.001$.

3.5. *miR-486-5p inhibited SRSF3 expression by binding with its 3′ UTR*

To investigate the target of miR-486-5p, we first predicted it by intersecting three types of genes, including the top 10 targets from the TargetScan and miRWalk databases and the top 10 hub genes in TCGA-LIHC dataset. Notably, only SRSF3 expression was detected (Fig. 6A). Pearson's correlation analysis indicated that miR-486-5p and SRSF3 expressions were negatively correlated (Fig. 6B). In HepG2 and Huh7 cells, *SRSF3* mRNA levels decreased following miR-486-5p overexpression (Fig. 6C). We then predicted the binding sites of miR-486-5p and SRSF3 (Fig. 6D) and validated them using a luciferase reporter assay (Fig. 6E).

3.6. *SRSF3 expression in TCGA-LIHC and CPTAC-HCC datasets*

We explored the relationship between SRSF3 expression and the clinicopathological characteristics of TCGA-LIHC dataset (Table 2). Differential expression analysis revealed higher SRSF3 expression in tumor tissues than in normal tissues in TCGA-LIHC dataset (Fig. 7A and B). Moreover, its expression was further increased in patients with HCC with several clinical features, including weight <70 kg (Fig. 7C), tumor (Fig. 7D), higher T stage (Fig. 7E), pathologic stage III (Fig. 7F), histologic grade G3 (Fig. 7G), vascular invasion (Fig. 7H), and AFP >400 ng/mL (Fig. 7I). Except for these, no difference was observed in SRSF3 expression among patients with different adjacent hepatic tissue inflammation (Fig. S5A), age (Fig. S5B), albumin (Fig. S5C), BMI (Fig. S5D), Child-Pugh grade (Fig. S5E), fibrosis ishak score (Fig. S5F), sex (Fig. S5G), height (Fig. S5H), N stage (Fig. S5I), prothrombin time (Fig. S5J), race (Fig. S5K), and residual tumor (Fig. S5L). In the CPTAC-HCC dataset, SRSF3 expression was higher in tumor tissues (Fig. S6A), whereas it was similar between male and female patients (Fig. S6B) and among patients of different ages (Fig. S6C).

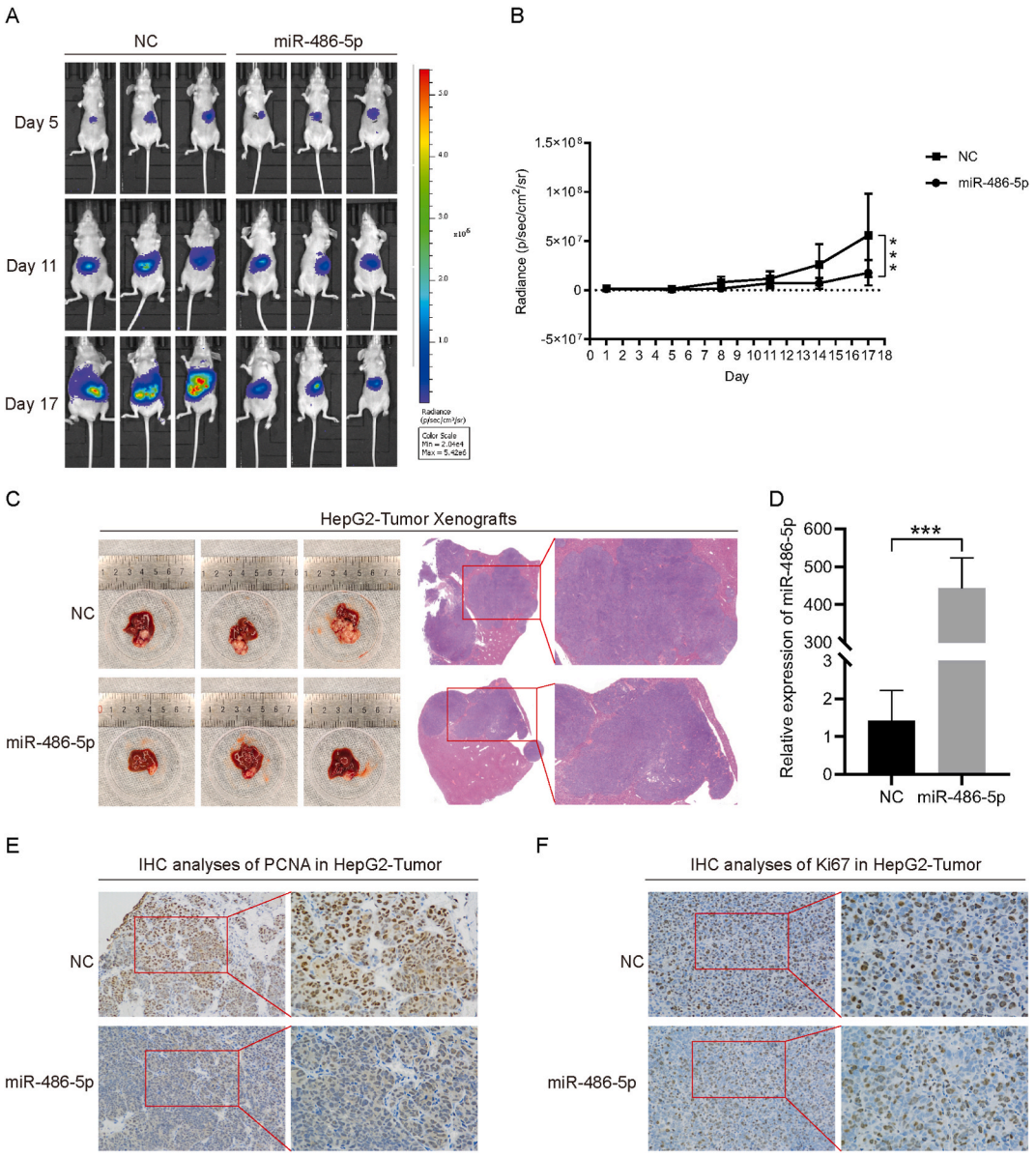

Fig. 5. miR-486-5p overexpression inhibited HCC growth *in vivo*.
(A, B) Tumor fluorescence intensity detected using *in vivo* bioluminescence imaging in nude mice injected with HepG2 cells transfected with miR-486-5p lentivirus expressing luciferase under the liver envelope. (C) Representative morphological and HE-stained HCC sections. (D) miR-486-5p expression in HCC tissues in the NC group and the miR-486-5p group. (E) IHC staining of PCNA in HCC tissues in the NC and miR-486-5p groups. (F) IHC staining of Ki67 in the HCC tissues in the NC and miR-486-5p groups. ***$p < 0.001$.

3.7. Clinical significance of SRSF3

In TCGA-LIHC dataset, the ROC curve showed an AUC of 0.821, indicating that SRSF3 expression could differentiate patients with HCC from healthy individuals (Fig. 8A). In terms of survival, higher SRSF3 expression predicted poorer overall survival (Fig. 8B and C) and disease-free survival (Fig. 8D and E).

3.8. SRSF3 functions

To predict SRSF3 functions in TCGA-LIHC dataset, we divided all samples into SRSF3 high- and low-expression groups. The DEGs between these two groups were analyzed, and an enrichment analysis was performed. GO analysis revealed that SRSF3 was differentially enriched in major BPs (such as liver development and RNA splicing), CCs (such as the exon-exon junction complex and

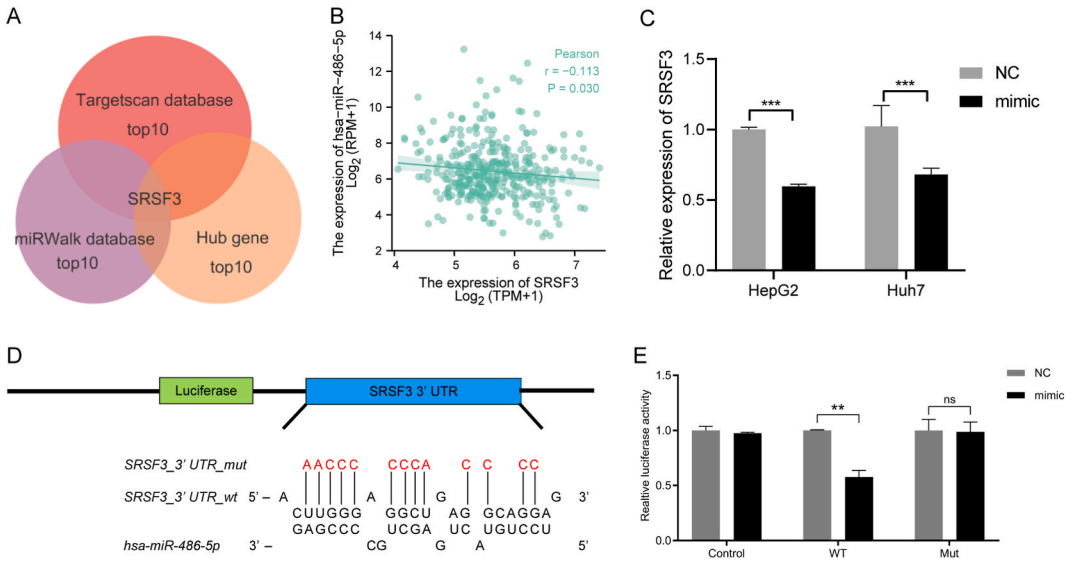

Fig. 6. Prediction and validation of the miR-486-5p target.
(A) The miR-486-5p target was predicted by intersecting the potential top 10 targets collected from Targetscan and miRWalk databases and the top 10 hub genes in TCGA-LIHC dataset. (B) The correlation between miR-486-5p and SRSF3 was determined using Pearson's analysis. (C) mRNA expression of *SRSF3* after miR-486-5p overexpression detected using qPCR. (D) The binding site between miR-486-5p and SRSF3. (E) The binding of miR-486-5p and SRSF3 detected using a luciferase reporter assay. **p < 0.01; ns, no significance.

transcription export complex), and MFs (such as pre-mRNA intronic and G-rich strand telomeric DNA binding) (Fig. 9A–C). KEGG pathway analysis showed that the spliceosome, mRNA surveillance pathway, RNA transport, and herpes simplex infection were significantly enriched in SRSF3-related DEGs (Fig. 9D). In addition, GSEA was performed to distinguish between the pathways that may be regulated by SRSF3 high- and low-expression groups. The SRSF3 high-expression group was significantly enriched in several signaling pathways, such as the cell cycle (Fig. 10A), focal adhesion (Fig. 10B), JAK–STAT signaling pathway (Fig. 10C), MAPK signaling pathway (Fig. 10D), NOTCH signaling pathway (Fig. 10E), p53 signaling pathway (Fig. 10F), several cancer pathways (Fig. 10G), TGF-β signaling pathway (Fig. 10H), and WNT signaling pathway (Fig. 10I).

3.9. Effects of miR-486-5p and SRSF3 on immune infiltration

The results of the CIBERSORT algorithm revealed that miR-486-5p expression was positively correlated with the degree of infiltration of multiple immune cells in HCC tissues (Figs. S7A and C). The effects of SRSF3 on immune cell infiltration were complex. Notably, its expression was positively correlated with the degree of infiltration of T helper (Th)2 cells, Th cells, TFH, NK CD56bright cells, aDC, Th1 cells, and macrophages, and negatively correlated with the degree of infiltration of Th17 cells, Treg cells, neutrophils, cytotoxic cells, pDC, and DC (Figs. S7B and D).

4. Discussion

With the rise of clinical big data in recent years, an increasing number of studies have been conducted to screen cancer biomarkers and therapeutic targets using bioinformatics methods. This study revealed the role of miR-486-5p by mining HCC-related datasets from TCGA and GEO databases. Notably, miR-486-5p inhibited HCC cell proliferation, migration, and invasion *in vitro* and suppressed HCC tumor growth *in vivo*. Its target, SRSF3, was predicted to be carcinogenic and was confirmed to be inhibited by miR-486-5p through binding to its 3' UTR.

miRNAs are a class of non-coding RNAs that are closely associated with HCC development [25]. In this study, we explored the correlation between miR-486-5p expression in HCC tissues and clinicopathological indicators in patients with HCC. Our analysis revealed no significant correlation between hsa-miR-486-5p expression and most clinicopathological characteristics. However, we observed a statistically significant correlation with the histological grade ($p = 0.042$). Specifically, patients with high hsa-miR-486-5p expression exhibited a higher proportion of G1 histological grade tumors (10 %) than those with low expression (4.9 %). Therefore, higher hsa-miR-486-5p expression was associated with lower histological grades, indicating a less aggressive tumor phenotype. Conversely, lower hsa-miR-486-5p expression was associated with more advanced histological grades (G3 and G4), supporting its role as a tumor suppressor miRNA in HCC. Additionally, a near-significant difference was observed for the residual tumor status ($p = 0.082$) and adjacent hepatic tissue inflammation ($p = 0.076$), suggesting potential trends that warrant further investigation.

Our findings are consistent with those of previous studies that explored miR-486-5p role in HCC. For instance, miR-486-5p was quantified in the serum of 116 patients with HCC and was associated with a lower risk of recurrence [26]. Additionally, Huang et al.

Table 2
Correlation between SRSF3 and clinicopathologic characteristics in patients with HCC.

Characteristic	Low expression of SRSF3	High expression of SRSF3	p-value
N	187	187	
T stage, n (%)			0.104
T1	101 (27.2 %)	82 (22.1 %)	
T2	46 (12.4 %)	49 (13.2 %)	
T3	31 (8.4 %)	49 (13.2 %)	
T4	6 (1.6 %)	7 (1.9 %)	
N stage, n (%)			0.624
N0	121 (46.9 %)	133 (51.6 %)	
N1	1 (0.4 %)	3 (1.2 %)	
M stage, n (%)			1.000
M0	130 (47.8 %)	138 (50.7 %)	
M1	2 (0.7 %)	2 (0.7 %)	
Pathologic stage, n (%)			0.094
Stage I	95 (27.1 %)	78 (22.3 %)	
Stage II	45 (12.9 %)	42 (12 %)	
Stage III	33 (9.4 %)	52 (14.9 %)	
Stage IV	3 (0.9 %)	2 (0.6 %)	
Tumor status, n (%)			0.026
Tumor free	111 (31.3 %)	91 (25.6 %)	
With tumor	65 (18.3 %)	88 (24.8 %)	
Gender, n (%)			0.185
Female	54 (14.4 %)	67 (17.9 %)	
Male	133 (35.6 %)	120 (32.1 %)	
Race, n (%)			0.086
Asian	70 (19.3 %)	90 (24.9 %)	
Black or African American	6 (1.7 %)	11 (3 %)	
White	100 (27.6 %)	85 (23.5 %)	
Age, n (%)			0.133
≤60	81 (21.7 %)	96 (25.7 %)	
>60	106 (28.4 %)	90 (24.1 %)	
Weight, n (%)			0.005
≤70	80 (23.1 %)	104 (30.1 %)	
>70	96 (27.7 %)	66 (19.1 %)	
Height, n (%)			0.265
< 170	97 (28.4 %)	104 (30.5 %)	
≥170	77 (22.6 %)	63 (18.5 %)	
BMI, n (%)			0.291
≤25	85 (25.2 %)	92 (27.3 %)	
>25	87 (25.8 %)	73 (21.7 %)	
Residual tumor, n (%)			0.902
R0	167 (48.4 %)	160 (46.4 %)	
R1	8 (2.3 %)	9 (2.6 %)	
R2	1 (0.3 %)	0 (0 %)	
Histologic grade, n (%)			0.001
G1	33 (8.9 %)	22 (6 %)	
G2	102 (27.6 %)	76 (20.6 %)	
G3	46 (12.5 %)	78 (21.1 %)	
G4	4 (1.1 %)	8 (2.2 %)	
Adjacent hepatic tissue inflammation, n (%)			0.013
None	71 (30 %)	47 (19.8 %)	
Mild	44 (18.6 %)	57 (24.1 %)	
Severe	13 (5.5 %)	5 (2.1 %)	
AFP(ng/mL), n (%)			<0.001
≤400	131 (46.8 %)	84 (30 %)	
>400	16 (5.7 %)	49 (17.5 %)	
Albumin(g/dl), n (%)			0.580
<3.5	40 (13.3 %)	29 (9.7 %)	
≥3.5	123 (41 %)	108 (36 %)	
Prothrombin time, n (%)			0.096
≤4	105 (35.4 %)	103 (34.7 %)	
>4	55 (18.5 %)	34 (11.4 %)	
Child-Pugh grade, n (%)			0.560
A	126 (52.3 %)	93 (38.6 %)	
B	10 (4.1 %)	11 (4.6 %)	
C	1 (0.4 %)	0 (0 %)	
Fibrosis ishak score, n (%)			0.126
0	49 (22.8 %)	26 (12.1 %)	
1/2	14 (6.5 %)	17 (7.9 %)	

(*continued on next page*)

Table 2 (*continued*)

Characteristic	Low expression of SRSF3	High expression of SRSF3	p-value
3/4	14 (6.5 %)	14 (6.5 %)	
5/6	40 (18.6 %)	41 (19.1 %)	
Vascular invasion, n (%)			0.491
No	112 (35.2 %)	96 (30.2 %)	
Yes	54 (17 %)	56 (17.6 %)	

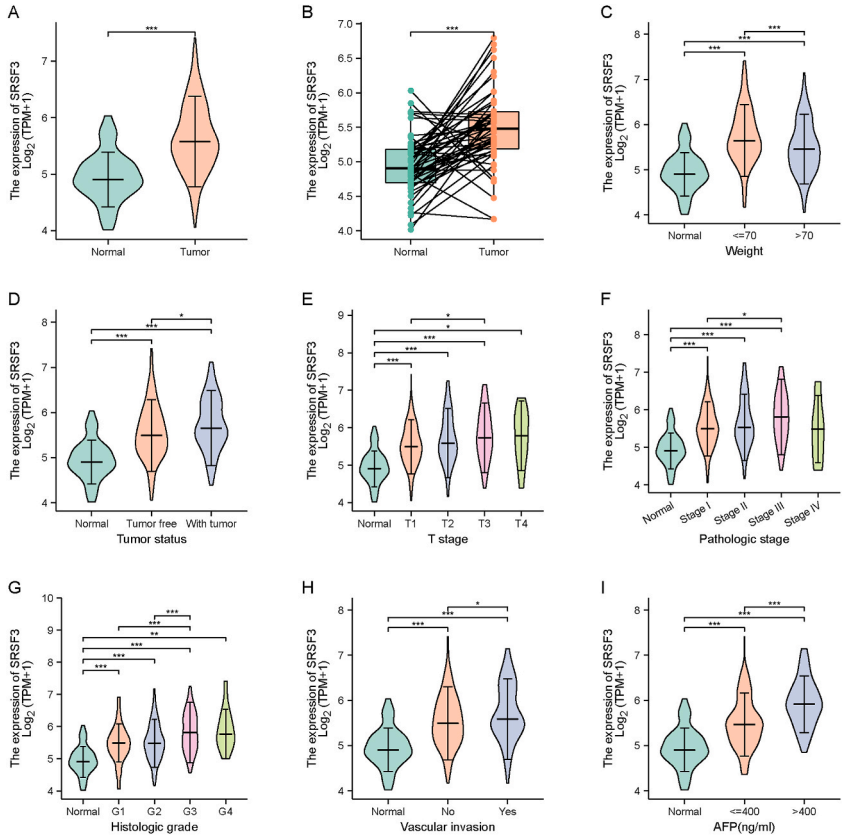

Fig. 7. SRSF3 expression in TCGA-LIHC dataset.
(A, B) SRSF3 expression in tumor and normal tissues of HCC. (C–I) The SRSF3 expression in patients with various clinical characteristics, including weight (C), tumor status (D), T stage (E), pathologic stage (F), histologic grade (G), vascular invasion (H), and AFP (I). *p < 0.05; **p < 0.01; ***p < 0.001.

confirmed decreased miR-486-5p levels in HCC tissues and seven HCC cell lines and identified PIK3R1 as a direct target of miR-486-5p [27]. Further studies have demonstrated that miR-486-5p can be sequestered by DLGAP1-AS1 [28] and Circ-TCF4.85 [29], which induce HCC cell proliferation by targeting H3F3B and ABCF2. Moreover, forced miR-486-5p expression represses cell proliferation via the insulin-like growth factor 1 receptor (IGF-1R) and downstream mediators mTOR, STAT3, and c-Myc [30]. Moreover, IGF-1R and its ligand, IGF-1, are downregulated by miR-486-5p in Huh7 cells [31]. By targeting SIRT1, miR-486-5p significantly suppresses self-renewal and tumorigenesis in liver CSCs [32]. CBL has also been reported as a miR-486-5p target in HCC [33].

In this study, we identified SRSF3 as a novel target of miR-486-5p, expanding the spectrum of miR-486-5p targets. SRSF3, a RNA-binding protein, is involved in the alternative splicing of mRNA and regulation of gene transcription and translation [34]. In cancer, it regulates processes such as cell proliferation, autophagy, and apoptosis [35,36]. The function of SRSF3 in HCC is complex and multifaceted. For example, SRSF3 stabilizes CCDC50S mRNA and enhances the oncogenic progression of HCC [37]. Additionally, SRSF3 switches PKM to PKM2 under the guidance of LNCAROD, thereby activating glycolysis and enhancing HCC malignancy [38]. However, Kumar et al. analyzed frozen human HCC samples and revealed increased mRNA expression but decreased protein expression of SRSF3 [39]. Furthermore, hepatocyte-specific SRSF3 knockout mice developed chronic liver damage and HCC. These reports have demonstrated contradictory results regarding the role of SRSF3. In addition to protein content, post-translational modifications of SRSF3 can also affect its function. Notably, dephosphorylation of SRSF3 contributes to the growth and invasion of HCC cells, accelerating their malignant transformation [40]. In our study, although we did not perform experimental studies on SRSF3

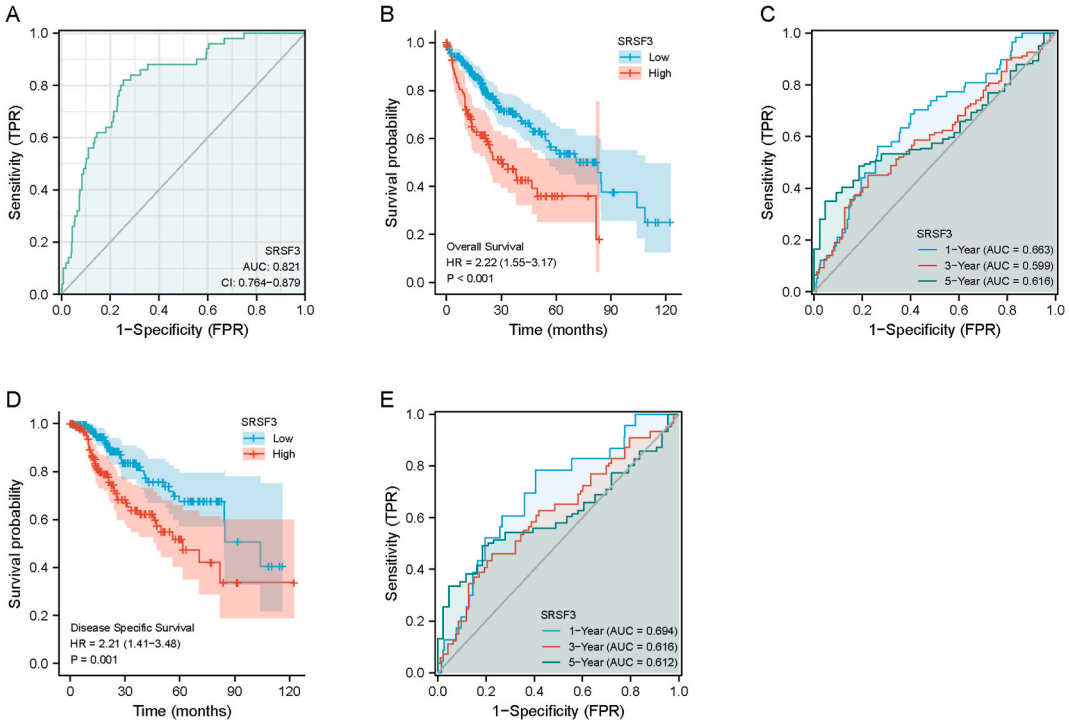

Fig. 8. Clinical significance of SRSF3 in TCGA-LIHC dataset.
(A) The diagnostic value of SRSF3 evaluated based on the ROC curve. (B) The effect of SRSF3 on overall survival evaluated using Cox regression in TCGA-LIHC dataset. (C) Time-dependent ROC curve evaluating the predictive efficacy of SRSF3 on overall survival. (D) The effect of SRSF3 on disease-specific survival evaluated using Cox regression in TCGA-LIHC dataset. (E) Time-dependent ROC curve evaluating the predictive efficacy of SRSF3 on disease-specific survival.

function, we found that *SRSF3* mRNA was upregulated in HCC tissues in TCGA-LIHC dataset. Patients with HCC and high *SRSF3* mRNA expression showed poor overall and disease-specific survival. The results of the enrichment analysis of SRSF3-related differentially expressed genes suggested an ambiguous role for SRSF3 in HCC, in contrast to the clear anti-cancer role of miR-486-5p. We conjecture that the performance of the SRSF3 may be model-dependent. Therefore, further investigation is warranted in this regard.

This study had some limitations. First, public data on serum miR-486-5p expression in patients with HCC remains unavailable. Future studies should explore whether miR-486-5p can serve as a novel molecular diagnostic marker. Although our results show that miR-486-5p is an anti-cancer miRNA in HCC, the mechanism underlying its low expression in HCC remains unclear, except for two reports on a competing endogenous RNA mechanism [28,29]. We hypothesized that genetic or epigenetic factors contribute to the low miR-486-5p expression in HCC. miR-486-5p is located on chromosome 8p11.21, an area rich in potential tumor suppressor genes, and deletions in this region are frequent in some types of cancer [41,42]. In addition, the promoter of the host gene for miR-486 is highly methylated in osteosarcoma cell lines [43], suggesting that DNA methylation and histone deacetylation may be involved in miR-486-5p downregulation in HCC. Furthermore, our study demonstrated a binding relationship between miR-486-5p and *SRSF3* mRNA *in vitro* using a luciferase reporter assay. We did not perform *in vivo* binding analyses or measure binding constants and thermodynamic parameters, which limits our understanding of the precise molecular interactions. This limitation aligns with the methodologies discussed by Rezaei et al., who provide a comprehensive approach to binding analysis that we recommend for future research [44]. Moreover, whether miR-486-5p exerts its anti-cancer effects solely through SRSF3 remains undetermined. The functions of SRSF3 have not been validated in other datasets or in cell and animal models. Notably, all of these inferences require validation in future experiments.

5. Conclusions

This study revealed that miR-486-5p may be involved in the development of HCC as a tumor suppressor miRNA based on bioinformatics approaches and assays, and miR-486-5p could be a potential diagnostic marker, prognostic indicator, and therapeutic target in HCC.

CRediT authorship contribution statement

Xiang Li: Data curation, Formal analysis, Methodology, Validation, Visualization, Writing – original draft, Writing – review &

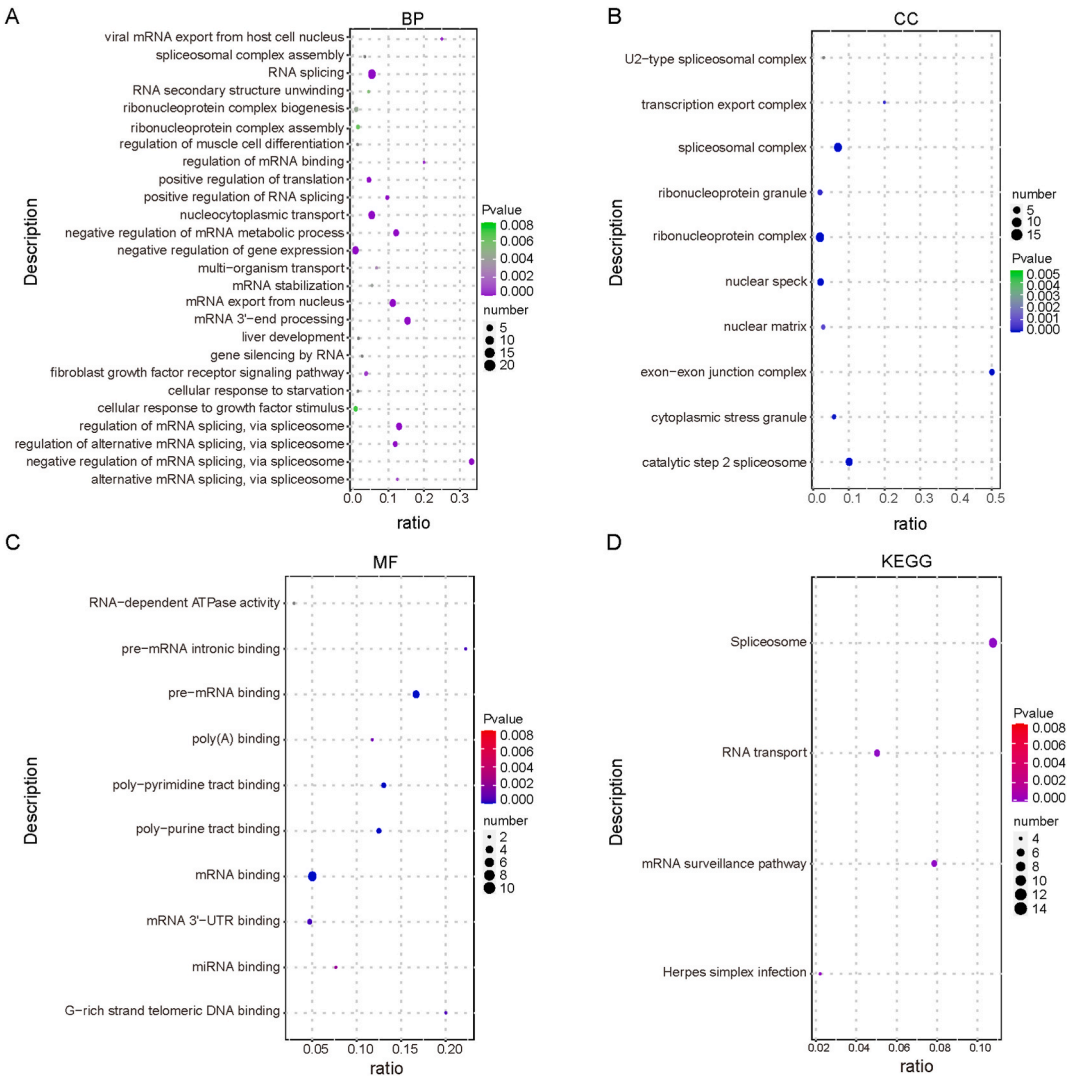

Fig. 9. SRSF3 functions predicted using GO and KEGG enrichment analyses.
The samples in TCGA-LIHC dataset were divided into high- and low-expression groups according to SRSF3 expression. DEGs between the two groups were subjected to GO-BP (A), GO-CC (B), GO-MF (C), and KEGG (D) enrichment analyses.

editing. **Jie Fang:** Conceptualization, Data curation, Investigation, Methodology, Resources, Writing – original draft, Writing – review & editing. **Xueyan Huang:** Conceptualization, Methodology, Writing – original draft, Writing – review & editing. **Yeqi Wu:** Investigation, Resources, Writing – original draft, Writing – review & editing. **Rui Wang:** Conceptualization, Funding acquisition, Project administration, Supervision, Writing – original draft, Writing – review & editing.

Data availability statement

Data will be made available on request.

Funding

Not applicable.

Declaration of competing interest

The authors declare that they have no known competing financial interests or personal relationships that could have appeared to influence the work reported in this paper.

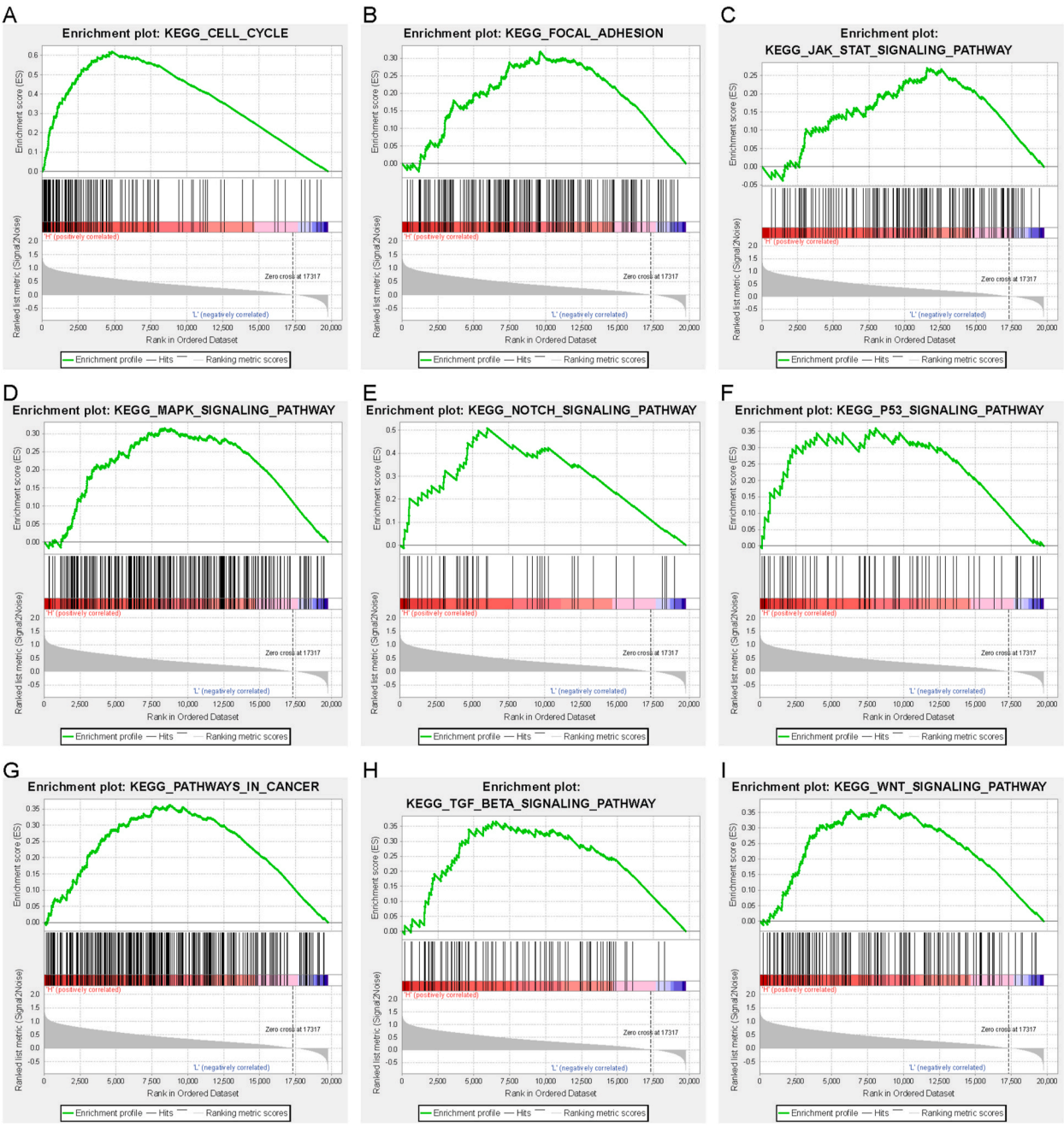

Fig. 10. SRSF3 functions predicted using GSEA.
The samples in TCGA-LIHC dataset were divided into high- and low-expression groups according to SRSF3 expression. (A–I) DEGs between the two groups were subjected to GSEA.

Abbreviations

miRNAs	MicroRNAs
HCC	hepatocellular carcinoma
TCGA	The Cancer Genome Atlas
GEO	Gene Expression Omnibus
SRSF3	Ser/Arg-rich splicing factor 3
AFP	Alpha-fetoprotein
CPTAC	Clinical Proteomic Tumor Analysis Consortium

DEMs	differentially expressed miRNAs
ROC:	receiver operating characteristic
KEGG	Kyoto Encyclopedia of Genes and Genomes
FBS	fetal bovine serum
qPCR	Quantitative polymerase chain reaction
CCK-8	Cell counting kit-8
HRP	horseradish peroxidase
HE	Hematoxylin-eosin
IHC	Immunohistochemical
BSA	bovine serum albumin
GO	Gene Ontology
BP	biological processes
CC	cellular components
MF	molecular function
GSEA	Gene Set Enrichment Analysis
Th	T helper
IGF-1R	insulin-like growth factor 1 receptor

Appendix A. Supplementary data

Supplementary data to this article can be found online at https://doi.org/10.1016/j.heliyon.2024.e39909.

References

[1] S. Chidambaranathan-Reghupaty, P.B. Fisher, D. Sarkar, Hepatocellular carcinoma (HCC): epidemiology, etiology and molecular classification, Adv. Cancer Res. 149 (2021) 1–61.
[2] X. Chi, et al., Targeted arsenite-loaded magnetic multifunctional nanoparticles for treatment of hepatocellular carcinoma, Nanotechnology 30 (17) (2019) 175101.
[3] T.X. Lu, M.E. Rothenberg, MicroRNA, J. Allergy Clin. Immunol. 141 (4) (2018) 1202–1207.
[4] Z. Ali Syeda, et al., Regulatory mechanism of MicroRNA expression in cancer, Int. J. Mol. Sci. 21 (5) (2020).
[5] S. Swarbrick, et al., Systematic review of miRNA as biomarkers in Alzheimer's disease, Mol. Neurobiol. 56 (9) (2019) 6156–6167.
[6] J.S. Hulot, N. Masurkar, miRNA-based therapeutics for heart failure: why not? J. Am. Coll. Cardiol. 75 (15) (2020) 1801–1803.
[7] Z. Tian, et al., Identification of important modules and biomarkers in breast cancer based on WGCNA, OncoTargets Ther. 13 (2020) 6805–6817.
[8] R.M. Komoll, et al., MicroRNA-342-3p is a potent tumour suppressor in hepatocellular carcinoma, J. Hepatol. 74 (1) (2021) 122–134.
[9] M. Hill, N. Tran, miRNA interplay: mechanisms and consequences in cancer, Dis Model Mech 14 (4) (2021).
[10] R. Lowe, et al., Transcriptomics technologies, PLoS Comput. Biol. 13 (5) (2017) e1005457.
[11] M. Moro, et al., MiR-486-5p targets CD133+ lung cancer stem cells through the p85/AKT pathway, Pharmaceuticals 15 (3) (2022).
[12] A. Pisano, et al., The Inhibitory Role of miR-486-5p on CSC Phenotype Has Diagnostic and Prognostic Potential in Colorectal Cancer. Cancers (Basel) 12 (11) (2020).
[13] B. Mansoori, et al., The synergy between miR-486-5p and tamoxifen causes profound cell death of tamoxifen-resistant breast cancer cells, Biomed. Pharmacother. 141 (2021) 111925.
[14] M.I. Love, W. Huber, S. Anders, Moderated estimation of fold change and dispersion for RNA-seq data with DESeq2, Genome Biol. 15 (12) (2014) 550.
[15] M.E. Ritchie, et al., Limma powers differential expression analyses for RNA-sequencing and microarray studies, Nucleic Acids Res. 43 (7) (2015) e47.
[16] D.S. Chandrashekar, et al., UALCAN: a portal for facilitating tumor subgroup gene expression and survival analyses, Neoplasia 19 (8) (2017) 649–658.
[17] X. Robin, et al., pROC: an open-source package for R and S+ to analyze and compare ROC curves, BMC Bioinf. 12 (2011) 77.
[18] H.Y. Huang, et al., miRTarBase 2020: updates to the experimentally validated microRNA-target interaction database, Nucleic Acids Res. 48 (D1) (2020) D148–D154.
[19] T. Wu, et al., clusterProfiler 4.0: a universal enrichment tool for interpreting omics data, Innovation 2 (3) (2021) 100141.
[20] Y. Xiong, et al., Icaritin ameliorates hepatic steatosis via promoting fatty acid beta-oxidation and insulin sensitivity, Life Sci. 268 (2021) 119000.
[21] C. Gene Ontology, The gene Ontology (GO) project in 2006, Nucleic Acids Res. 34 (Database issue) (2006) D322–D326.
[22] J. Du, et al., KEGG-PATH: Kyoto encyclopedia of genes and genomes-based pathway analysis using a path analysis model, Mol. Biosyst. 10 (9) (2014) 2441–2447.
[23] A. Liberzon, et al., The Molecular Signatures Database (MSigDB) hallmark gene set collection, Cell Syst 1 (6) (2015) 417–425.
[24] S. Hanzelmann, R. Castelo, J. Guinney, GSVA: gene set variation analysis for microarray and RNA-seq data, BMC Bioinf. 14 (2013) 7.
[25] K. Oura, A. Morishita, T. Masaki, Molecular and functional roles of MicroRNAs in the progression of hepatocellular carcinoma-A review, Int. J. Mol. Sci. 21 (21) (2020).
[26] L. Wang, et al., Identification of recurrence-related serum microRNAs in hepatocellular carcinoma following hepatectomy, Cancer Biol. Ther. 16 (10) (2015) 1445–1452.
[27] X.P. Huang, et al., MicroRNA-486-5p, which is downregulated in hepatocellular carcinoma, suppresses tumor growth by targeting PIK3R1, FEBS J. 282 (3) (2015) 579–594.
[28] X. Peng, F. Wei, X. Hu, Long noncoding RNA DLGAP1-AS1 promotes cell proliferation in hepatocellular carcinoma via sequestering miR-486-5p, J. Cell. Biochem. 121 (2) (2020) 1953–1962.
[29] J. Gao, et al., Circ-TCF4.85 silencing inhibits cancer progression through microRNA-486-5p-targeted inhibition of ABCF2 in hepatocellular carcinoma, Mol. Oncol. 14 (2) (2020) 447–461.
[30] R.A. Youness, et al., MicroRNA-486-5p enhances hepatocellular carcinoma tumor suppression through repression of IGF-1R and its downstream mTOR, STAT3 and c-Myc, Oncol. Lett. 12 (4) (2016) 2567–2573.
[31] R.A. Youness, et al., Contradicting interplay between insulin-like growth factor-1 and miR-486-5p in primary NK cells and hepatoma cell lines with a contemporary inhibitory impact on HCC tumor progression, Growth Factors 34 (3–4) (2016) 128–140.

[32] X. Yan, et al., MicroRNA-486-5p functions as a tumor suppressor of proliferation and cancer stem-like cell properties by targeting Sirt1 in liver cancer, Oncol. Rep. 41 (3) (2019) 1938–1948.
[33] J. He, et al., MiR-486-5p suppresses proliferation and migration of hepatocellular carcinoma cells through downregulation of the E3 ubiquitin ligase CBL, BioMed Res. Int. 2019 (2019) 2732057.
[34] D.A. More, A. Kumar, SRSF3: newly discovered functions and roles in human health and diseases, Eur. J. Cell Biol. 99 (6) (2020) 151099.
[35] Z. Zhou, et al., Emerging roles of SRSF3 as a therapeutic target for cancer, Front. Oncol. 10 (2020) 577636.
[36] Y. Che, L. Fu, Aberrant expression and regulatory network of splicing factor-SRSF3 in tumors, J. Cancer 11 (12) (2020) 3502–3511.
[37] H. Wang, et al., A coiled-coil domain containing 50 splice variant is modulated by serine/arginine-rich splicing factor 3 and promotes hepatocellular carcinoma in mice by the ras signaling pathway, Hepatology 69 (1) (2019) 179–195.
[38] G. Jia, et al., LNCAROD enhances hepatocellular carcinoma malignancy by activating glycolysis through induction of pyruvate kinase isoform PKM2, J. Exp. Clin. Cancer Res. 40 (1) (2021) 299.
[39] D. Kumar, et al., Hepatocyte deletion of IGF2 prevents DNA damage and tumor formation in hepatocellular carcinoma, Adv. Sci. 9 (21) (2022) e2105120.
[40] D. Chen, et al., PPM1G promotes the progression of hepatocellular carcinoma via phosphorylation regulation of alternative splicing protein SRSF3, Cell Death Dis. 12 (8) (2021) 722.
[41] H.K. Oh, et al., Genomic loss of miR-486 regulates tumor progression and the OLFM4 antiapoptotic factor in gastric cancer, Clin. Cancer Res. 17 (9) (2011) 2657–2667.
[42] J. Wang, et al., Downregulation of miR-486-5p contributes to tumor progression and metastasis by targeting protumorigenic ARHGAP5 in lung cancer, Oncogene 33 (9) (2014) 1181–1189.
[43] H.M. Namlos, et al., miR-486-5p expression is regulated by DNA methylation in osteosarcoma, BMC Genom. 23 (1) (2022) 142.
[44] S. Rezaei, et al., Investigation on the effect of fluorescence quenching of calf thymus DNA by piperine: caspase activation in the human breast cancer cell line studies, DNA Cell Biol. 43 (1) (2024) 26–38.